IEEE Access
Multidisciplinary | Rapid Review | Open Access Journal

Received January 9, 2019, accepted January 21, 2019, date of publication February 5, 2019, date of current version February 27, 2019.

Digital Object Identifier 10.1109/ACCESS.2019.2897693

Disturbance Rejection of IPMSM Drives by Simplified Taylor Series-Based Near Optimal Control Scheme in Wide Speed Range

MUHAMMAD SAAD RAFAQ, ANH TUAN NGUYEN, HAN HO CHOI, (Member, IEEE), AND JIN-WOO JUNG, (Member, IEEE)
Division of Electronics and Electrical Engineering, Dongguk University, Seoul 04620, South Korea

Corresponding author: Jin-Woo Jung (jinwjung@dongguk.edu)

This work was supported by the Basic Science Research Program through the National Research Foundation of Korea (NRF) funded by the Ministry of Education under Grant 2018R1D1A1B07046873.

ABSTRACT This paper proposes a simplified near optimal control (NOC) scheme to reject the disturbances of interior permanent magnet synchronous motor (IPMSM) drives by minimizing the complex calculations in the Taylor series method required for solving the state-dependent Riccati equation (SDRE). Since the speed tracking performance of an IPMSM can be significantly degraded in the presence of the disturbances owing to the practical factors (e.g., external load torque, parameter uncertainties, and so on), an SDRE-based near optimal disturbance observer (NODO) is designed to accurately estimate and reject the disturbances associated with the speed and current in the feedforward control. The state-dependent coefficient matrices of the IPMSM are rearranged in the controller and observer to minimize the complex offline calculations of the Taylor series method used to solve the SDRE. By significantly simplifying the calculations, the proposed SDRE-based NOC scheme can be efficiently applied to the IPMSM drives. To verify the precise and robust control performance of the proposed NODO-based near optimal speed controller, experiments are conducted via a prototype IPMSM drive system with a TI-TMS320F28335 DSP under different disturbances. Finally, the comparative experimental results with the conventional NOC are presented under load change and wide speed range conditions.

INDEX TERMS Interior permanent magnet synchronous motor (IPMSM), near optimal disturbance observer (NODO), near optimal speed controller (NOSC), state-dependent Riccati equation (SDRE), Taylor series method.

I. INTRODUCTION

High efficiency, simple structure, high power density, and wide speed range operation are the advantageous traits of the interior permanent magnet synchronous motor (IPMSM) which encourages its application to the electric vehicles, robotics, aerospace, and other industrial fields [1]–[4]. In these industrial applications, the IPMSM drives require the precise speed control during transient and steady-state under various operating conditions [5]. Nevertheless, in the real-time applications, the speed control performance of the IPMSM deteriorates due to the presence of the unwanted disturbances [6] such as external load torque, motor parameter variations, and unmodeled dynamics (e.g., dead-time effect, current measurement sensor errors, etc.) [7]. In particular, the sudden change in the external load torque directly affects the desired dq-axis current references, which disturbs the stable rotor speed in the steady-state and then leads to the large transient speed tracking errors [8], [9]. Meanwhile, the motor parameter variations (e.g., stator resistance, d-q axis inductances, magnet flux linkage, rotor inertia, viscous friction coefficient, etc.) are mainly caused by the temperature, magnetic saturation, and ageing of the motor [10]. The mismatch between the nominal values and actual values of the motor parameters can worsen the tracking control performance because this control design requires the accurate knowledge of the motor parameters [11]. In order to achieve the precise speed control during transient and steady-state

The associate editor coordinating the review of this manuscript and approving it for publication was Zhong Wu.

operations in the presence of different disturbances, numerous linear optimal and nonlinear near optimal control techniques [12]–[20] are reported in the literature to attenuate the effects of the disturbances.

Among linear optimal control techniques designed for the precise speed control of IPMSM drives, the linear quadratic regulator (LQR) based control [13] is particularly applied by considering the tradeoff between input control efforts and transient response. However, the negative effects of the disturbances are not properly attenuated by the LQR control owing to the constant parameters of the Riccati equation which can highly degrade the transient and steady-state tracking performance of the IPMSM drives [14]. On the other hand, the nonlinear near optimal control design is reported in terms of the state-dependent Riccati equation (SDRE) control framework [15], which can be called a nonlinear system version of the LQR control. The near optimal control can utilize the nonlinear system model directly in the LQR-like optimal control design, by first bringing the system to a state-dependent coefficient (SDC) linear structure [16]. Also, the optimal gains obtained by solving the state-dependent algebraic Riccati equation (ARE) provide the design flexibility in the SDRE control [17]. The key problem regarding the SDRE based nonlinear control is to calculate the solution of the SDRE which requires a lot of computational efforts. In [18], Schur decomposition is applied to solve the Hamiltonian matrix of the SDRE, which cannot be performed in case of the complex nonlinear system dynamics. Similarly, the complex iterative algorithms to solve the SDRE require the fast sampling time to ensure the system stability during SDRE iterations. In [19], the speed control for the permanent magnet synchronous motor (PMSM) is designed such that the SDRE solution is obtained from the Taylor series numerical technique. In [20], the Taylor series technique for calculating the SDRE solution is further extended to design the good speed tracking controller of the IPMSM drives in the presence of the reluctance torque and nonlinearities. However, the state-dependent matrices [19], [20] are complex, which require many computations to calculate the solution of the SDRE. Hence, in order to enhance the applicability of the SDRE based approach, much emphasis is put on simplifying the computation methods without compromising the precise speed control of the IPMSM.

In order to reduce the complex computations in the Taylor series for solving the SDRE, this paper proposes a simplified near optimal control (NOC) scheme for IPMSM drives. Besides, an SDRE-based near optimal disturbance observer (NODO) is proposed to estimate and then compensate for the disturbances (e.g., external load torque, parameter variations, unmodeled dynamics, etc.) encountered in the IPMSM during the practical implementations. In the simplified SDRE-based NOC (i.e., both the controller and disturbance observer (DO)), the state-dependent coefficients of the IPMSM are restructured in order to minimize the complex calculations in Taylor series method. The approximate solutions of the SDREs for the proposed near optimal speed controller (NOSC) and NODO are easily calculated offline by solving one constant ARE and a series of constant Lyapunov equations (CLEs). In order to prove the effectiveness of the proposed NOC technique, experiments are carried out on a prototype IPMSM drive system with a TI TMS320F28335 DSP for the load change and wide speed range conditions in the presence of the disturbances. The comparative experimental results with the conventional NOC scheme [20] are presented to clearly highlight the efficacy of the proposed technique.

A. DYNAMIC MODEL OF AN IPMSM

In the $d-q$ reference frame rotating synchronously at the electrical rotor speed ω_r, the electrical and mechanical dynamics of an IPMSM can be derived as the following differential equations [21]:

$$\begin{aligned}\frac{di_{qs}}{dt} &= \frac{1}{L_q}\left(v_{qs} - R_s i_{qs} - \lambda_m \omega_r - L_d \omega_r i_{ds}\right)\\ \frac{di_{ds}}{dt} &= \frac{1}{L_d}\left(v_{ds} - R_s i_{ds} + L_q \omega_r i_{qs}\right)\\ \frac{d\omega_r}{dt} &= \frac{p}{2J}\left(\tau_e - \frac{2B}{p}\omega_r - \tau_L\right)\\ \tau_e &= 1.5\frac{p}{2}\left(\lambda_m i_{qs} + \Delta L_{dq} i_{ds} i_{qs}\right)\end{aligned} \tag{1}$$

where τ_e is the electromagnetic torque, τ_L is the load torque considered as an unknown disturbance that changes slowly during a small sampling period (T_s), p is the number of poles, R_s is the stator resistance, L_d and L_q are the d-axis and q-axis inductances, ΔL_{dq} is the $L_d - L_q$, J is the rotor inertia, B is the viscous friction coefficient, λ_m is the magnet flux linkage, i_{ds} and i_{qs} are the d-axis and q-axis stator currents, and v_{ds} and v_{qs} are the d-axis and q-axis voltages, respectively. To facilitate the design of the SDRE-based controller, the parameters of the IPMSM model (1) can be reduced as

$$\begin{aligned}&l_1 = 1.5\frac{1}{J}\frac{p^2}{4}\lambda_m, \quad l_2 = \frac{B}{J}, \quad l_3 = \frac{p}{2J}, \quad l_4 = \frac{R_s}{L_q},\\ &l_5 = \frac{\lambda_m}{L_q}, \quad l_6 = \frac{1}{L_q}, \quad l_7 = \frac{R_s}{L_d}, \quad l_8 = \frac{1}{L_d}, \quad l_9 = \frac{L_q}{L_d},\\ &l_{10} = \frac{L_d}{L_q}, \quad l_{11} = 1.5\frac{1}{J}\frac{p^2}{4}\Delta L_{dq}.\end{aligned} \tag{2}$$

And the disturbances, i.e., external load torque (τ_L), parameter uncertainties ($\Delta l_1, \ldots, \Delta l_{11}$), and unstructured uncertainties due to the unmodeled dynamics (i.e., ε_ω, ε_q, and ε_d that represent the dead-time effects, current measurement sensor errors, etc.) of the IPMSM are lumped together as

$$\begin{aligned}d &= \begin{bmatrix} d_\omega \\ d_q \\ d_d \end{bmatrix}\\ &= \begin{bmatrix} \Delta l_1 i_{qs} - \Delta l_2 \omega_r - (l_3 + \Delta l_3)\tau_L + \Delta l_{11} i_{ds} i_{qs} + \varepsilon_\omega \\ -\Delta l_4 i_{qs} - \Delta l_5 \omega_r - \Delta l_{10} \omega_r i_{ds} + \Delta l_6 v_q + \varepsilon_q \\ -\Delta l_7 i_{ds} + \Delta l_8 v_d + \Delta l_9 \omega_r i_{qs} + \varepsilon_d \end{bmatrix}.\end{aligned} \tag{3}$$

Since this paper is not aimed at minimizing the torque ripples, the high-order harmonics and cogging torque are not specified in the ε_ω, ε_q, and ε_d. And by utilizing (2)−(3), the IPMSM model (1) becomes

$$\frac{d}{dt}\begin{bmatrix}\omega_r\\ i_{qs}\\ i_{ds}\end{bmatrix}=\begin{bmatrix}l_1 i_{qs}-l_2\omega_r+l_{11}i_{ds}i_{qs}+d_\omega\\ -l_4 i_{qs}-l_5\omega_r-l_{10}\omega_r i_{ds}+d_q\\ -l_7 i_{ds}+l_9\omega_r i_{qs}+d_d\end{bmatrix}+\begin{bmatrix}0&0\\ l_6&0\\ 0&l_8\end{bmatrix}\begin{bmatrix}v_{qs}\\ v_{ds}\end{bmatrix}. \quad (4)$$

The nonlinear dynamics of the IPMSM presented in (4) is analogous to a general nonlinear system, i.e., $\dot{x}=f(x)+Bu$. Note that ω_r, i_{qs}, and i_{ds} in (4) are the state variables whose measurement information is available, and v_{qs} and v_{ds} are the control inputs. In the $d-q$ axis model of an IPMSM, the performance analysis for speed regulation is not intuitive in the nonlinear dynamics (4). In order to achieve the linearization of the nonlinear dynamics of the IPMSM and the state-dependent coefficient (SDC) form in (4), it is preferable to define the state tracking errors as

$$e_\omega=\omega_r-\omega_d,\quad e_{iq}=i_{qs}-i_{qsd},\quad e_{id}=i_{ds}-i_{dsd}, \quad (5)$$

where ω_d is the desired rotor speed, e_ω is the rotor speed error, i_{qsd} and i_{dsd} are the desired q-axis and d-axis currents, and e_{iq} and e_{id} are the q-axis and d-axis current errors, respectively. It is noted that the desired speed ω_d changes slowly with respect to a small sampling period (T_s). Then, by applying the state errors (5) to the speed equation in (4), the desired q-axis current (i_{qsd}) can be obtained as

$$i_{qsd}=\left(l_2\omega_d+\dot{\omega}_d-d_\omega-l_{11}i_{dsd}i_{qs}\right)/(l_1+l_{11}e_{id}). \quad (6)$$

Next, the desired d-axis current (i_{dsd}) in the IPMSM drives to operate in the wide speed range is determined by two types of the d-axis stator currents: i_{dsd_MTPA} by the maximum torque per ampere (MTPA) control below the rated speed (ω_{rated}) and i_{dsd_FW} by the flux-weakening (FW) control above the rated speed (ω_{rated}) [22]. Thus, the wide speed range operation for an IPMSM can be achieved by setting the i_{dsd} as

$$i_{dsd}=(1-n)\,i_{dsd\_MTPA}+n\,i_{dsd\_FW} \quad (7a)$$

where

$$\begin{aligned} n(\omega_r)&=\begin{cases}0, & \omega_r\le\omega_{rated}\\ 1, & \omega_r>\omega_{rated}\end{cases}\\ i_{dsd\_MTPA}&=\frac{l_{10}-1}{l_5}\,i_{qs}^2\\ i_{dsd\_FW}&=-l_9\left(l_5-\frac{l_6\,V_m}{\omega_r}+\frac{\omega_r\,i_{qs}^2}{2l_6\,V_m}\right)\\ V_m&\ge v_{ds}^2+v_{qs}^2. \end{aligned} \quad (7b)$$

And V_m is limited by the dc-link voltage (V_{dc}), i.e., $V_m=V_{dc}/\sqrt{3}$. Therefore, a stabilizing feedback control (i.e., a simplified SDRE-based NOSC) is designed in Section III to implement the wide speed range operation for an IPMSM drive under different operating conditions. Next, the disturbances of the IPMSM are estimated by the simplified SDRE-based NODO and then compensated for in the feedforward control. Meanwhile, Table 1 presents the list of acronyms used in this paper to improve its readability.

TABLE 1. List of acronyms.

Acronym	Abbreviation
ARE	Algebraic Riccati Equation
CLE	Constant Lyapunov Equation
FW	Flux-Weakening
IPMSM	Interior Permanent Magnet Synchronous Motor
LQR	Linear Quadratic Regulator
MTPA	Maximum Torque Per Ampere
NOC	Near Optimal Control
NODO	Near Optimal Disturbance Observer
NOSC	Near Optimal Speed Controller
SDC	State-Dependent Coefficient
SDRE	State-Dependent Riccati Equation
SSE	Steady-State Error

II. SIMPLIFIED NEAR OPTIMAL SPEED CONTROLLER DESIGN WITH REDUCED CALCULATIONS OF TAYLOR SERIES METHOD FOR SDRE SOLUTION

This section designs a simplified SDRE-based NOSC and a simplified Taylor series method is addressed to solve the SDRE for the near optimal control (NOC).

A. SIMPLIFIED SDRE-BASED NOSC DESIGN

An SDRE is a simple extension of the constant-valued algebraic Riccati equation (ARE) used to find the feedback control law in the LQR. In this section, the extensive calculations required to solve the SDRE are minimized by appropriately selecting the SDC form of the IPMSM model. Since many SDC parameterizations are possible, the most appropriate SDC should be selected to design the control law that keeps the control objectives. Therefore, the control input $U_{dq}=[v_{qs},v_{ds}]^T$ is divided into the following two terms:

$$U_{dq}=\begin{bmatrix}v_{qs}\\ v_{ds}\end{bmatrix}=u_{FF}+u_{FB}-d_{dq} \quad (8)$$

where $u_{FF}=[u_{FFq},u_{FFd}]^T$ represents the dq-axis feedforward terms of the IPMSM which are directly compensated and defined as

$$\begin{aligned} u_{FF}&=\begin{bmatrix}\frac{1}{l_6}\left(l_4 i_{qsd}+l_5\omega_d+\dot{i}_{qsd}+l_{10}(e_{id}\omega_d+\omega_r i_{dsd}+e_{id}e_\omega)\right)\\ \frac{1}{l_8}\left(l_7 i_{dsd}+\dot{i}_{dsd}-l_9 e_{iq}\omega_d-l_9\omega_r i_{qsd}-l_9 e_{iq}e_\omega\right)\end{bmatrix}\\ &=\begin{bmatrix}u_{FFq}\\ u_{FFd}\end{bmatrix} \end{aligned} \quad (9)$$

$u_{FB}=[u_{FBq},u_{FBd}]^T$ represents the dq-axis feedback terms of the IPMSM which are stabilized by the NOSC design, respectively, and $d_{dq}=[d_q/l_6,\,d_d/l_8]^T$ represents the unknown disturbances. Note that the d_q and d_d in the U_{dq} are the unknown

disturbances estimated by the NODO to be presented in the next section. Then, the error dynamics of the IPMSM by using (4)−(9) can be written as

$$\underbrace{\begin{bmatrix}\dot{e}_\omega\\ \dot{e}_{iq}\\ \dot{e}_{id}\end{bmatrix}}_{\dot{x}} = \underbrace{\begin{bmatrix}-l_2 & l_1 & l_{11}e_{iq}\\ -l_5 & -l_4 & 0\\ 0 & 0 & -l_7\end{bmatrix}}_{A(x)} \underbrace{\begin{bmatrix}e_\omega\\ e_{iq}\\ e_{id}\end{bmatrix}}_{x} + \underbrace{\begin{bmatrix}0 & 0\\ l_6 & 0\\ 0 & l_8\end{bmatrix}}_{B} \underbrace{\begin{bmatrix}u_{FBq}\\ u_{FBd}\end{bmatrix}}_{u_{FB}}. \tag{10}$$

The stabilizing near optimal feedback control (NOFC) law for the error dynamics (10) is given by

$$u_{FB} = -\Lambda(x)x = -T^{-1}B^T\Gamma(x)x \tag{11}$$

which is obtained by minimizing the following quadratic performance cost function:

$$J(x, u_{FB}) = \frac{1}{2}\int_{t_0}^{\infty}\left(x^TQx + u_{FB}^TTu_{FB}\right)\,dt \tag{12}$$

where $Q \in \boldsymbol{R}^{3\times3}$ is a constant symmetric positive semi-definite weighting matrix, $T \in \boldsymbol{R}^{2\times2}$ is a constant symmetric positive definite weighting matrix, $\Lambda(x)$ is a gain matrix, and $\Gamma(x) \in \boldsymbol{R}^{3\times3}$ is a unique, symmetric, and positive definite solution of the following SDRE:

$$\Gamma(x)A(x) + A^T(x)\Gamma(x) - \Gamma(x)BT^{-1}B^T\Gamma(x) + Q = 0. \tag{13}$$

The gain matrix $\Lambda(x)$ of (11) can be evaluated by finding the $\Gamma(x)$ of the SDRE (13) such that the equilibrium of the closed-loop system is asymptotically stable [23]. Note that the $\Gamma(x)$ and $A(x)$ are the state-dependent parameters to imply that the NOC law (11) is also state-dependent. Now, consider the following constant-valued ARE:

$$\Gamma_0A_0 + A_0^T\Gamma_0 - \Gamma_0BT^{-1}B^T\Gamma_0 + Q = 0 \tag{14}$$

where A_0 and Γ_0 are the constant matrices to imply that the Λ_0 will also be a constant matrix. In this regard, $A(x)$ can be rewritten as the following:

$$\underbrace{\begin{bmatrix}-l_2 & l_1 & l_{11}e_{iq}\\ -l_5 & -l_4 & 0\\ 0 & 0 & -l_7\end{bmatrix}}_{A(x)} = \underbrace{\begin{bmatrix}-l_2 & l_1 & 0\\ -l_5 & -l_4 & 0\\ 0 & 0 & -l_7\end{bmatrix}}_{A_0} + \underbrace{\begin{bmatrix}0 & 0 & l_{11}e_{iq}\\ 0 & 0 & 0\\ 0 & 0 & 0\end{bmatrix}}_{\tilde{A}(x)} \tag{15}$$

and $\Gamma(x) = \Gamma_0 + \Delta\Gamma(x)$ and $\Lambda(x) = \Lambda_0 + \Delta\Lambda(x)$. $\tilde{A}(x)$, $\Delta\Gamma(x)$, and $\Delta\Lambda(x)$ are the state-dependent incremental matrices. Γ_0 is the solution of the (14) such that $\Lambda_0 = T^{-1}B^T\Gamma_0$ and $\Delta\Lambda(x) = T^{-1}B^T\Delta\Gamma(x)$. Then, the NOC law (11) becomes

$$u_{FB} = -\left(\Lambda_0 + \Delta\Lambda(x)\right)x. \tag{16}$$

By putting (16) into (10), the following state-space equation is derived:

$$\dot{x} = \left(A_0 - B\Lambda_0\right)\,x + \left(\Delta A(x) - B\Delta\Lambda(x)\right)\,x. \tag{17}$$

Note that the solution of the SDRE (13) is very critical and requires many computations. Based on these issues, the notable efforts should be made to simplify the Taylor series method for solving the SDRE (13).

B. SIMPLIFIED TAYLOR SERIES METHOD FOR SOLVING SDRE

In this section, the Taylor series expansion is employed to approximately calculate the solution of the SDRE (13). In this regard, the $A(x)$ in (15) is rewritten as

$$A(x) = A_0 + \sigma\tilde{A}(x) \tag{18}$$

where σ is the temporary variable utilized to represent the Taylor series and after completing the series derivation, the value of σ will be set to 1. The Taylor series expansion for solving the SDRE (13) is expressed by

$$\begin{aligned}\Gamma(x,\sigma) &= \Gamma(x)|_{\sigma=0} + \left.\frac{\partial\Gamma(x)}{\partial\sigma}\right|_{\sigma=0}\sigma + \left.\frac{\partial^2\Gamma(x)}{\partial\sigma^2}\right|_{\sigma=0}\frac{\sigma^2}{2}\ldots\\ &= \sum_{n=0}^{\infty}\sigma^n\Gamma_n(x)\end{aligned} \tag{19}$$

where each $\Gamma_n(x)$ is symmetric because $\Gamma(x)$ is symmetric. The state-dependent incremental matrix $\tilde{A}(x)$ can be rewritten by using the constant matrix A_{Cq} and variable e_{iq}.

$$\tilde{A}(x) = e_{iq}\underbrace{\begin{bmatrix}0 & 0 & l_{11}\\ 0 & 0 & 0\\ 0 & 0 & 0\end{bmatrix}}_{\Delta A_{Cq}}. \tag{20}$$

By inserting (20) into (19), the Taylor series expansion is rewritten as

$$\Gamma(x,\sigma) = \sum_{n=0}^{\infty}\sigma^n e_{iq}^n\Gamma_n^C \tag{21}$$

where each Γ_n^C is a constant matrix. Substituting (18) and (20)−(21) into (13) yields the following equation (22.a) presented at the bottom of the next page. Based on (21), the $\Gamma(x)$ in (13) can be written as $e_{iq}^n\Gamma_n^C$ and the e_{iq}^n can be omitted from (22.a). The (22.b), as shown at the bottom of the next page, is an expanded form of the (22.a) with the omitted e_{iq}^n. The like powers of σ in (22.b), which is an expanded form of the (22.a) with e_{iq}^n, are rearranged to formulate the iterative method that finds the Γ_n^C matrices while the coefficients are set to zero below. For σ^0:

$$\Gamma_0^CA_0 + A_0^T\Gamma_0^C - \Gamma_0^CBT^{-1}B^T\Gamma_0^C + Q = 0 \tag{23}$$

For σ^1:

$$\begin{aligned}&\Gamma_1^C\left(A_0 - BT^{-1}B^T\Gamma_0^C\right) + \left(A_0 - BT^{-1}B^T\Gamma_0^C\right)^T\Gamma_1^C\\ &\quad + \Gamma_0^C\Delta A_{Cq} + \Delta A_{Cq}^T\Gamma_0^C = 0\\ &\quad\vdots\end{aligned} \tag{24}$$

For σ^n:

$$\Gamma_n^C\left(A_0 - BT^{-1}B^T\Gamma_0^C\right) + \left(A_0 - BT^{-1}B^T\Gamma_0^C\right)^T\Gamma_n^C + \Gamma_{(n-1)}^C\Delta A_{Cq} + \Delta A_{Cq}^T\Gamma_{(n-1)}^C - \sum_{j=1}^{n-1}\Gamma_j^C BT^{-1}B^T\Gamma_{(n-j)}^C = 0 \tag{25}$$

where the 3 ×3 matrix Γ_0^C is the solution of (23) which is analogous to the ARE (14). Meanwhile, $\Gamma_1^C \ldots \Gamma_n^C$ are the solutions of the constant Lyapunov equations (CLEs). The iteration method (23)−(25) approximately converges to the solution of the SDRE (13) because $A(x)$ is continuous and B is constant [24]. This indicates that the $\Gamma(x)$ can be approximated by the Γ_n^C $(n = 0, 1, \ldots, N)$ which is calculated by one constant ARE and a series of CLEs.

Thus, the stabilizing NOFC law (11) becomes

$$u_{FB} = -\left(T^{-1}B^T\sum_{n=0}^{N}e_{iq}^n\Gamma_n^C\right)x = -\left(\sum_{n=0}^{N}e_{iq}^n\Lambda_n\right)x \tag{26}$$

where $\Lambda_n = T^{-1}B^T\Gamma_n^C$ is the gain matrix and N is the number of members of the Taylor series calculated offline. Fig. 1 presents the block diagram of the proposed SDRE-based NOSC with reduced calculations of Taylor series method.

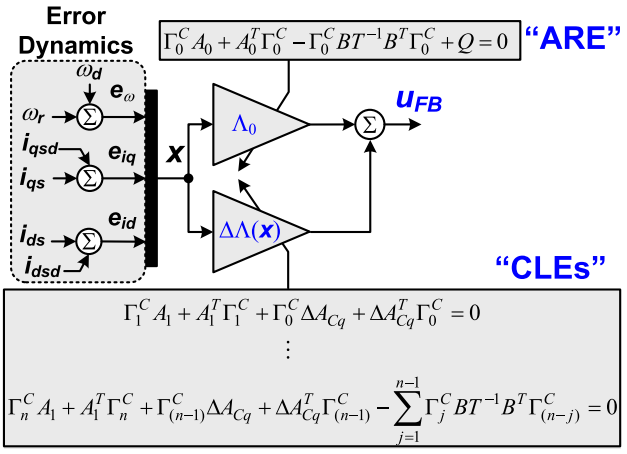

FIGURE 1. Block diagram of the proposed SDRE-based NOSC with reduced calculations of Taylor series method.

III. SIMPLIFIED NEAR OPTIMAL DISTURBANCE OBSERVER DESIGN AND OBSERVER-BASED SPEED CONTROLLER

This section designs a simplified SDRE-based NODO to estimate the disturbances of an IPMSM and then these estimated disturbances are utilized in the feedforward compensation terms to minimize the unwanted disturbances d.

A. SIMPLIFIED SDRE-BASED NODO DESIGN

The unwanted disturbances $d(t)$ in the IPMSM deteriorate the accurate tracking performance of the NOSC. Therefore, in order to enhance the accurate speed and current tracking performance of the IPMSM, the theory of SDRE is extended to the NODO design that can estimate the external disturbances and parameter uncertainties. It is assumed that the disturbances $d(t)$ vary slowly during a small sampling time (T_s) relative to the observer dynamics, i.e., $\dot{d}(t) \approx 0$ is employed to ensure the stability of the proposed SDRE-based NODO. The dynamic model (4) can be restructured to design the proposed disturbance observer as

$$\underbrace{\begin{bmatrix}\dot{d}\\ \dot{x}_{dob}\end{bmatrix}}_{\dot{x}_d} = \underbrace{\begin{bmatrix}\mathrm{O}_{3\times3} & \mathrm{O}_{3\times3}\\ \mathrm{I}_{3\times3} & A_{dob}(x_{dob})\end{bmatrix}}_{A_d(x_d)}\underbrace{\begin{bmatrix}d\\ x_{dob}\end{bmatrix}}_{x_d} + \underbrace{\begin{bmatrix}\mathrm{O}_{3\times1}\\ u_{dob}\end{bmatrix}}_{u_d} \tag{27}$$

where

$$A_{dob}(x_{dob}) = \begin{bmatrix}-l_2 & l_1 & l_{11}\,i_{qs}\\ -l_5 & -l_4 & 0\\ l_9\,i_{qs} & 0 & -l_7\end{bmatrix},\quad x_{dob} = \begin{bmatrix}\omega_r\\ i_{qs}\\ i_{ds}\end{bmatrix},$$

$$u_{dob} = \begin{bmatrix}0\\ -l_{10}\,i_{ds}\,\omega_r + l_6\,v_q\\ l_8\,v_d\end{bmatrix},$$

$I_{3\times3}$ and $\mathrm{O}_{3\times3}$ are the identity matrix and zero matrix with the relevant sizes (i.e., the subscript 3×3 means 3 rows and 3 columns), respectively, and the output y_d is given as

$$y_d = \underbrace{\begin{bmatrix}\mathrm{O}_{3\times3} & \mathrm{O}_{3\times3}\\ \mathrm{O}_{3\times3} & \mathrm{I}_{3\times3}\end{bmatrix}}_{C_d}x_d. \tag{28}$$

In order to design the NODO, the quadratic cost function is represented as

$$J_d(\hat{x}_d, \hat{u}_d) = \frac{1}{2}\int_{t_0}^{\infty}\left(\hat{x}_d^T Q_d\hat{x}_d + \hat{u}_d^T T_d\hat{u}_d\right)dt \tag{29}$$

where $Q_d \in \boldsymbol{R}^{6\times6}$ is a constant symmetric positive semidefinite weighting matrix, and $T_d \in \boldsymbol{R}^{6\times6}$ is a constant symmetric

$$\left(\sum_{n=0}^{\infty}\sigma^n e_{iq}^n\Gamma_n^C\right)\left(A_0+\sigma\, e_{iq}\,\Delta A_{Cq}\right)+\left(A_0+\sigma\, e_{iq}\,\Delta A_{Cq}\right)^T\left(\sum_{n=0}^{\infty}\sigma^n e_{iq}^n\Gamma_n^C\right)-\left(\sum_{n=0}^{\infty}\sigma^n e_{iq}^n\Gamma_n^C\right)BT^{-1}B^T\left(\sum_{n=0}^{\infty}\sigma^n e_{iq}^n\Gamma_n^C\right)+Q=0. \tag{22a}$$

$$\sigma^0\Gamma_0^C A_0 + \sigma^0 A_0^T\Gamma_0^C + \sigma\Gamma_1^C A_0 + \sigma A_0^T\Gamma_1^C + \sigma\Gamma_0^C\Delta A_{Cq} + \sigma\Delta A_{Cq}^T\Gamma_0^C + \cdots + \sigma^n\Gamma_n^C A_0 + \sigma^n A_0^T\Gamma_n^C + \sigma^n\Gamma_{(n-1)}^C\Delta A_{Cq} + \sigma^n\Delta A_{Cq}^T\Gamma_{(n-1)}^C - \left(\sigma^0\Gamma_0^C + \sigma\Gamma_1^C + \cdots + \sigma^n\Gamma_n^C\right)BT^{-1}B^T\left(\sigma^0\Gamma_0^C + \sigma\Gamma_1^C + \cdots + \sigma^n\Gamma_n^C\right) + Q = 0. \tag{22b}$$

positive definite weighting matrix. The associated dynamics of the NODO become

$$\dot{\hat{x}}_d = A_d^T(\hat{x}_d)\hat{x}_d + C_d^T\hat{u}_d \tag{30}$$

where $\hat{x}_d = [\hat{d}, \hat{x}_{ob}]^T$ is the estimate of x_d, and $\hat{u}_d \in \boldsymbol{R}^{6\times 1}$ is the control input vector. Then, the proposed NODO model can be expressed as

$$\begin{aligned}\dot{\hat{x}}_d &= A_d(\hat{x}_d)\hat{x}_d + u_d + L(\hat{x}_d)\left(y_d - C_d\hat{x}_d\right)\\ \hat{d} &= C_T\hat{x}_d\end{aligned} \tag{31}$$

where $\hat{d} = [\hat{d}_\omega, \hat{d}_q, \hat{d}_d]^T$ is the estimate of $d = [d_\omega, d_q, d_d]^T$ and $C_T = [\mathrm{I}_{3\times 3}, \mathrm{O}_{3\times 3}]$. The $\hat{d}(t)$ yielded by the NODO locally asymptotically converges to the d by employing the gain matrix given as

$$L(\hat{x}_d) = \Pi(\hat{x}_d)C_d^T T_d^{-1} \tag{32}$$

where $\Pi(\hat{x}_d)$ is the solution of the following SDRE:

$$A_d(\hat{x}_d)\Pi(\hat{x}_d) + \Pi(\hat{x}_d)A_d^T(\hat{x}_d) - \Pi(\hat{x}_d)C_d^T T_d^{-1}C_d\Pi(\hat{x}_d) + Q_d = 0. \tag{33}$$

The proposed NODO gain matrix $L(\hat{x}_d) \in \boldsymbol{R}^{6\times 6}$ is the near optimal solution of the optimal control problem (27) obtained by minimizing the quadratic cost function (29).

B. SIMPLIFIED TAYLOR SERIES METHOD FOR SOLVING SDRE

As presented in Section III, the state-dependent matrix $A_d(\hat{x}_d) \in \boldsymbol{R}^{6\times 6}$ can be rewritten as

$$\underbrace{\begin{bmatrix}\mathrm{O}_{3\times 3} & \mathrm{O}_{3\times 3}\\ \mathrm{I}_{3\times 3} & A_{ob}(\hat{x}_{dob})\end{bmatrix}}_{A_d(\hat{x}_d)} = \underbrace{\begin{bmatrix}\mathrm{O}_{3\times 3} & \mathrm{O}_{3\times 3}\\ \mathrm{I}_{3\times 3} & \bar{A}_{ob}\end{bmatrix}}_{A_{dC}} + \underbrace{\begin{bmatrix}\mathrm{O}_{3\times 3} & \mathrm{O}_{3\times 3}\\ \mathrm{O}_{3\times 3} & \Delta A_{dob}(\hat{x}_{dob})\end{bmatrix}}_{\Delta A_d(\hat{x}_d)} \tag{34}$$

where

$$A_{ob} = \begin{bmatrix}-l_2 & l_1 & 0\\ -l_5 & -l_4 & 0\\ 0 & 0 & -l_7\end{bmatrix},$$

$$\Delta A_{dob}(\hat{x}_{dob}) = \begin{bmatrix}0 & 0 & l_{11}\hat{i}_{qs}\\ 0 & 0 & 0\\ l_9\hat{i}_{qs} & 0 & 0\end{bmatrix},$$

A_{dC} is the constant matrix, and $\Delta A_d(\hat{x}_d)$ is the state-dependent incremental matrix that can be rewritten in the form of the constant matrix ΔA_{obCq} and variable $\hat{i}_{qs}$ as

$$\Delta A_d(\hat{x}_d) = \hat{i}_{qs}\underbrace{\begin{bmatrix}\mathrm{O}_{3\times 3} & \mathrm{O}_{3\times 3}\\ \mathrm{I}_{3\times 3} & \Delta A_{dobCq}\end{bmatrix}}_{\Delta A_{dCq}} \tag{35}$$

where $\Delta A_{dobCq} = \begin{bmatrix}0 & 0 & l_{10}\\ 0 & 0 & 0\\ l_8 & 0 & 0\end{bmatrix}$.

Similarly, $L(\hat{x}_d) = L_0 + \Delta L(\hat{x}_d)$; $\Pi(\hat{x}_d) = \Pi_0 + \Delta\Pi(\hat{x}_d) = \sum_{n=1}^{N_d}\hat{i}_{qs}^n\Pi_n^C$ provided that $L_0 = \Pi_0 C_d^T T_d^{-1}$ and $\Delta L(\hat{x}_d) = \Delta\Pi(\hat{x}_d)C_d^T T_d^{-1}$. Note that the matrices $\Pi_n^C \in \boldsymbol{R}^{6\times 6}$ are the constant matrices. Then, the iterative method for finding the $\Pi(\hat{x}_d)$ is presented by using the constant matrices Π_n^C as

$$A_{dC}\Pi_0^C + \Pi_0^C A_{dC}^T - \Pi_0^C C_d^T T_d^{-1}C_d\Pi_0^C + Q_d = 0 \tag{36}$$

$$\begin{aligned}&\left(A_{dC} - \Pi_0^C C_d^T T_d^{-1}C_d\right)\Pi_1^C + \Pi_1^C\left(A_{dC} - \Pi_0^C C_d^T T_d^{-1}C_d\right)^T\\ &\quad + \Pi_0^C\Delta A_{dCq}^T + \Delta A_{dCq}\Pi_0^C = 0\\ &\quad\vdots\end{aligned} \tag{37}$$

$$\begin{aligned}&\left(A_{dC} - \Pi_0^C C_d^T T_d^{-1}C_d\right)\Pi_n^C\\ &+ \Pi_n^C\left(A_{dC} - \Pi_0^C C_d^T T_d^{-1}C_d\right)^T\\ &+ \Pi_{(n-1)}^C\Delta A_{dCq}^T + \Delta A_{dCq}\Pi_{(n-1)}^C\\ &- \sum_{j=1}^{n-1}\Pi_j^C C_d^T T_d^{-1}C_d\Pi_{(n-j)}^C = 0\end{aligned} \tag{38}$$

where the 6 ×6 matrix Π_0 is the solution of the ARE (36) and $\Pi_1^C \ldots \Pi_n^C$ are the solution of the CLEs (37)−(38). Then, the gain matrix (32) can be presented as

$$L(\hat{x}_d) = \left(\sum_{n=1}^{N_d}\hat{i}_{qs}^n\Pi_n^C\right)C_d^T T_d^{-1} = \sum_{n=0}^{N_d}L_n\hat{i}_{qs}^n \tag{39}$$

where N_d is the number of members of the Taylor series calculated offline.

C. NODO-BASED NOSC DESIGN

Fig. 2 summarizes the design procedure for the proposed NODO-based NOSC. In this paper, the proposed simplified SDRE-based NOSC is designed under the assumption that the disturbances $d(t)$ are available. In other words, these disturbances $d(t)$ are estimated by the proposed NODO (31), and the desired q-axis current i_{qsd} (6) can be updated with the

❶ Initialization	Step I	Measure x and evaluate $A(x)$ and B.
	Step II	Choose Q, T, Q_d, and T_d via Bryson's Rule .
❷ SDRE Disturbance Observer	Step I	Solve ARE (36) for $\Pi_0{}^C$.
	Step II	Solve Lyapunov equation (37)–(38) for $\Pi_1{}^C \rightarrow \Pi_n{}^C$.
	Step III	Calculate Gain (39) for the disturbance observer.
❸ Update	Step I	Update $\hat{d}(t)$ to the i_{qsd} (40), u_{FF} (41), and U_{dq} (42).
❹ SDRE Speed Controller	Step I	Solve ARE (23) for $\Gamma_0{}^C$.
	Step II	Solve Lyapunov equation (24)–(25) for $\Gamma_1{}^C \rightarrow \Gamma_n{}^C$.
	Step III	Calculate (26) by using $\Gamma_0{}^C \rightarrow \Gamma_n{}^C$.
	Step IV	Combine u_{FF} and u_{FB} for the control input.

FIGURE 2. Design procedure for the proposed NODO-based NOSC.

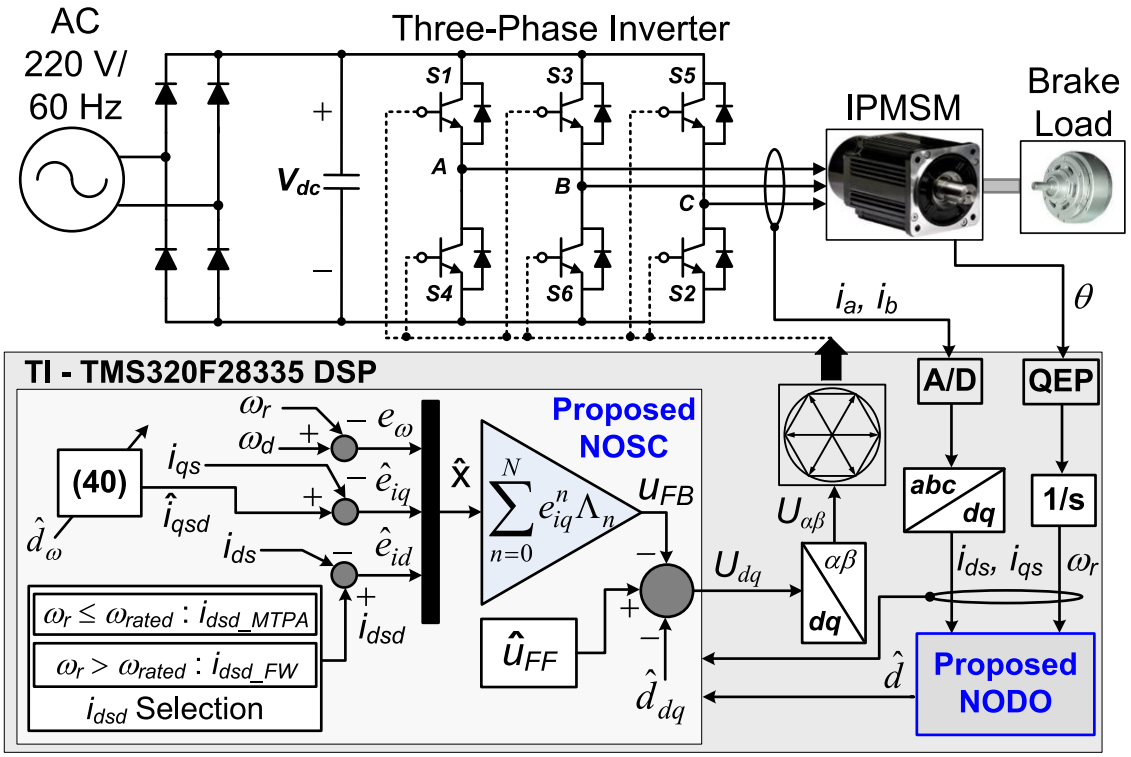

(a)

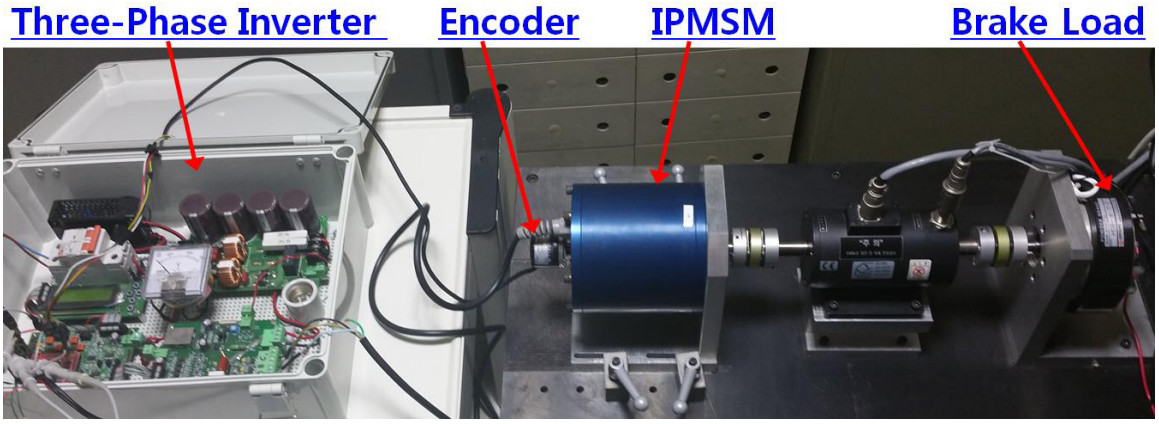

(b)

FIGURE 3. Experimental test-bench employed to implement the proposed NODO-based NOSC for an IPMSM drive. (a) Overall control block diagram. (b) Photograph of an IPMSM experimental test-bench.

following $\hat{i}_{qsd}$:

$$\hat{i}_{qsd} = \left(l_2\omega_d + \dot{\omega}_d - \hat{d}_\omega - l_{11}i_{dsd}i_{qs}\right) \Big/ (l_1 + l_{11}e_{id}) \quad (40)$$

And $\hat{e}_{iq} = i_{qs} - \hat{i}_{qsd}$; $\hat{x} = [e_\omega, \hat{e}_{iq}, e_{id}]^T$. By utilizing the $\hat{i}_{qsd}$ in (40), the feedforward terms u_{FF} in (9) are modified as

$$\hat{u}_{FF} = \begin{bmatrix} \frac{1}{l_6}\left(l_4\hat{i}_{qsd} + l_5\omega_d + \dot{\hat{i}}_{qsd} + l_{10}(e_{id}\omega_d + \omega_r i_{dsd} + e_{id}e_\omega)\right) \\ \frac{1}{l_8}\left(l_7 i_{dsd} + \dot{i}_{dsd} - l_9 e_{iq}\omega_d - l_9\omega_r\hat{i}_{qsd} - l_9\hat{e}_{iq}e_\omega\right) \end{bmatrix}. \quad (41)$$

The $\hat{d} = [\hat{d}_\omega, \hat{d}_q, \hat{d}_d]^T$ is also updated to the $d_{dq} = [d_q/l_6, d_d/l_8]^T$ and the control inputs of the proposed SDRE-based NOSC with reduced calculations of Taylor series method presented in (8) become

$$U_{dq} = -\left(\sum_{n=0}^{N} e_{iq}^n \Lambda_n\right)\hat{x} - \begin{bmatrix} \hat{d}_q/l_6 \\ \hat{d}_d/l_8 \end{bmatrix} + \hat{u}_{FF}. \quad (42)$$

Remark 1: The SDC presentation of the proposed NOSC (26) is arranged so that the $\Delta A(x)$ is simply based on only one variable for solving the Taylor series, i.e., e_{iq} which can significantly minimize the computations required. On the

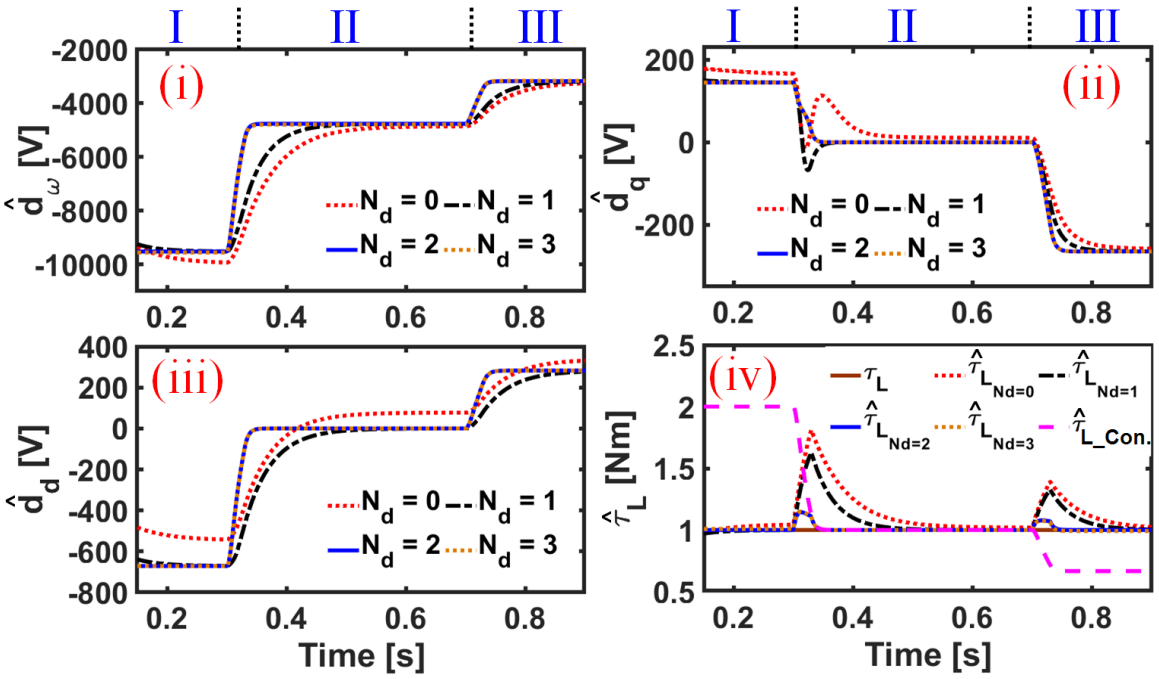

FIGURE 4. Comparative robust tracking evaluation of the proposed NODO ($\hat{d} = [\hat{d}_\omega, \hat{d}_q, \hat{d}_d]^T$ for $N_d = 0$, 1, 2, and 3) and the conventional NODO ($\hat{\tau}_{L\_Con}$).

TABLE 2. Nominal parameters of an IPMSM experimental test-bench.

Quantity	Symbol	Value
q-axis inductance	L_{q0}	113.91[mH]
d-axis inductance	L_{d0}	74.98[mH]
Magnet flux linkage	λ_{m0}	0.193[V·s/rad]
Stator resistance	R_{s0}	2.48[Ω]
Viscous friction coefficient	B_0	0.0001[N·m·s/rad]
Equivalent rotor inertia	J_0	0.00042[kg·m^2]
PWM switching frequency	f_s	5[kHz]
Sampling period	T_s	200[μs]
dc-link voltage	V_{dc}	295[V]
Number of poles	p	4
Rated power	P_{rated}	390[W]
Rated phase current	I_{rated}	1.3[A]
Rated speed	ω_{rated}	523[rad/s]
Rated load torque	$\tau_{L-rated}$	1.5[N·m]

other hand, the SDC presentation of the conventional NOSC in [20] is designed such that the $\Delta A(x)$ requires two variables for solving the Taylor series, i.e., e_{iq} and e_{id}. In this way, the number of algebraic Lyapunov equations in the proposed NOSC method is reduced to half compared to [20]. Next, the proposed NODO is particularly designed to estimate and reject the disturbances such as external load torque (τ_L), parameter uncertainties ($\Delta l_1, \ldots, \Delta l_{11}$), and unstructured uncertainties due to the unmodeled dynamics. Also, the incremental matrix $\Delta A_d(\hat{x}_d)$ for the proposed NODO is based on only one variable, i.e.,$\hat{i}_{qs}$. However, the conventional NODO [20] only estimates the load torque disturbance (τ_L) and the other disturbances are left unattended. Meanwhile, the conventional NODO [20] can be extended to estimate the $d = [d_\omega, d_q, d_d]^T$. In this case, the state-dependent matrix $A_d(\hat{x}_d)$ in (34) can be represented by the following matrices:

$$\bar{A}_{ob} = \begin{bmatrix} -l_2 & l_1 & 0 \\ -l_5 & -l_4 & 0 \\ 0 & 0 & -l_7 \end{bmatrix},$$

$$\Delta A_{dob}(\hat{x}_{dob}) = \begin{bmatrix} 0 & 0 & l_{11}\hat{i}_{qs} \\ -l_{10}\hat{i}_{ds} & 0 & 0 \\ l_9\hat{i}_{qs} & 0 & 0 \end{bmatrix},$$

and the gain matrix of the updated conventional NODO [20] is $L(\hat{x}_d) = \sum_{n=0}^{N_d} L_n \hat{i}_{qs}^n \hat{i}_{ds}^{Nd-n}$. It is noted that the $L(\hat{x}_d)$ in the updated conventional NODO uses the two variables, i.e., $\hat{i}_{qs}$ and $\hat{i}_{ds}$ to calculate its gain matrix, which implies that the $L(\hat{x}_d)$ is calculated by solving the twice the number of CLEs compared with the proposed NODO (31). Hence, compared to [20], the proposed simplified NODO minimizes the calculations required to solve the Taylor series and rejects the disturbances on a wider scale by estimating $\hat{d} = [\hat{d}_\omega, \hat{d}_q, \hat{d}_d]^T$.

IV. EXPERIMENTAL VERIFICATIONS

This section presents the layout of the experimental test-bench used to validate the proposed NOC (i.e., NOSC and NODO). Next, experiments are conducted under the load and speed change conditions.

A. EXPERIMENTAL TEST-BENCH

To verify the feasibility and validity of the proposed NODO-based NOSC, experiments are performed on a prototype IPMSM drive. Fig. 3(a) and (b) presents the overall control block diagram and photograph of the IPMSM experimental test-bench in which TI TMS320F28335 DSP is

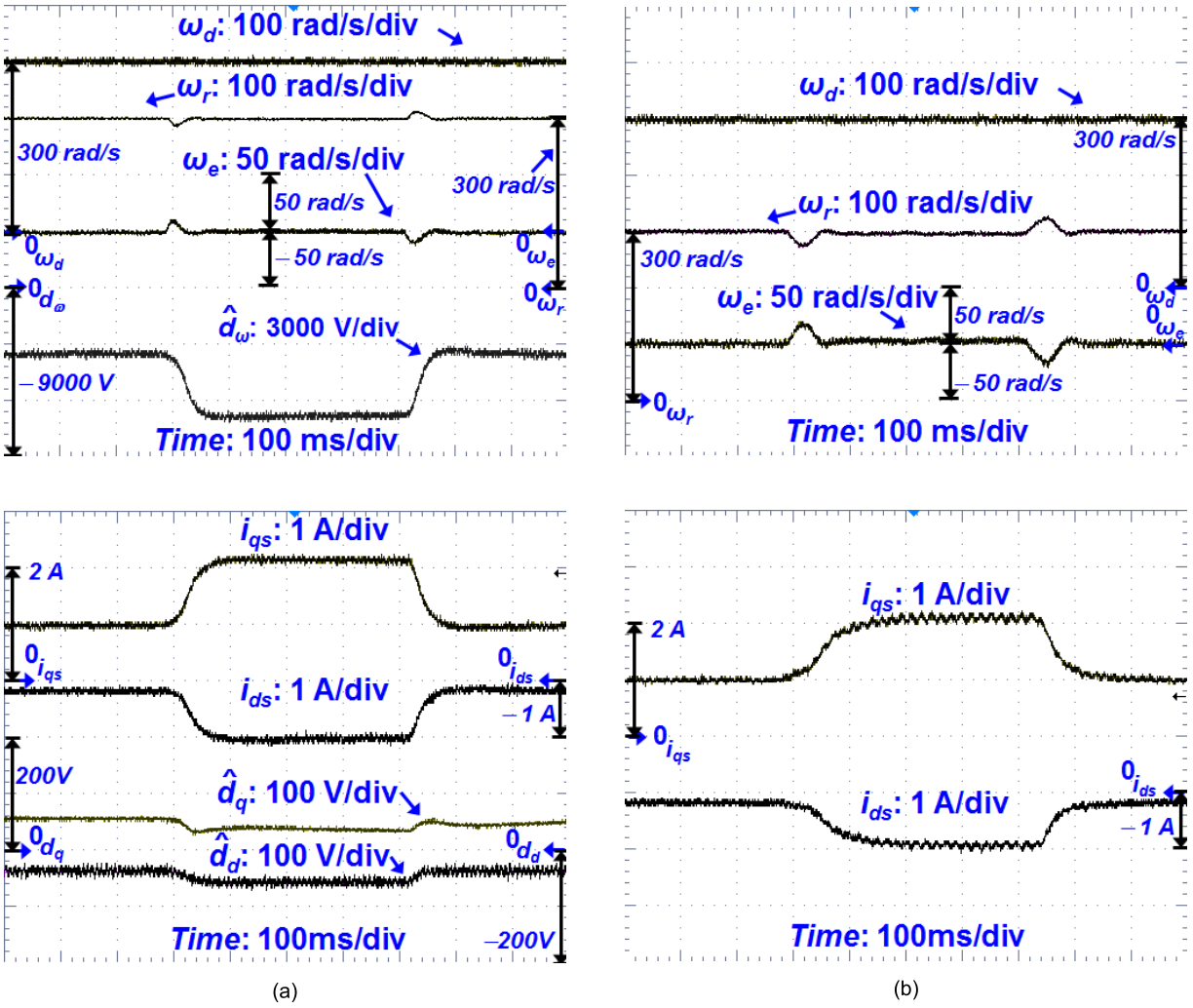

(a) (b)

FIGURE 5. Comparative experimental results under a load torque step change without parameter variations. (a) Proposed NOC ($\hat{d}_\omega$, $\hat{d}_q$, $\hat{d}_d$, ω_r, i_{ds}, and i_{qs}). (b) Conventional NOC (ω_r, i_{ds}, and i_{qs}).

employed to implement the proposed algorithm. As shown in Fig. 3(a), the three-phase currents (i_a, i_b) and rotor position angle (θ) are measured via Hall-effect current sensors and an incremental encoder with 2500 pulses per revolution scale, respectively. A magnetic powdered brake controlled via programmable variable dc supply is used to apply the external load torque disturbance. The nominal parameters for an IPMSM experimental test-bench are presented in Table 2. As illustrated in the design procedure of Fig. 2, the control weight matrices for the proposed NOSC and NODO are selected as: $Q = \text{diag}\ (2, 8, 8)$, $T = 0.001 \times \text{I}_{2\times2}$, $Q_d = \text{diag}\ (0.3, 5, 5, 85, 85, 90)$, and $T_d = 0.0001 \times \text{I}_{6\times6}$. Note that these weighting matrices highly affect the transient behavior of the system, so they are carefully tuned via Bryson's rule [25]. In this paper, the control input (v_{qs}, v_{ds}) generated from the proposed control algorithm is performed via a space vector pulse-width modulation (SVPWM) technique. For a fair comparison, the performance of the proposed NOC is compared with that of the conventional NOC [20] to highlight the rapid and stable speed response with a minimal overshoot, small settling time (t_s), and reduced steady-state error (SSE) under different operating conditions with parameter variations.

B. EVALUATION OF ROBUST TRACKING PERFORMANCE OF THE PROPOSED NODO WITH RESPECT TO N d

This subsection discusses the optimum number (N_d) of members of the Taylor series selected for the proposed NODO in view of the convergence rate, SSE, and computational burden. As presented in (39), the gain matrix $L(\hat{x}_d)$ of the proposed NODO is calculated by summing up the N_d calculated offline. For $N_d = 0$, $L(\hat{x}_d)$ is calculated only by solving the ARE (36), which can also be written as L_0. By increasing the N_d, the $L(\hat{x}_d)$ is calculated by solving (36)−(38) to find the solution of Π_n^C.

Fig. 4(i)−(iii) shows the estimated disturbances $\hat{d} = [\hat{d}_\omega, \hat{d}_q, \hat{d}_d]^T$ by the proposed NODO for $N_d = 0, 1, 2$, and 3 in the presence of the parameter variations. For a fair comparison

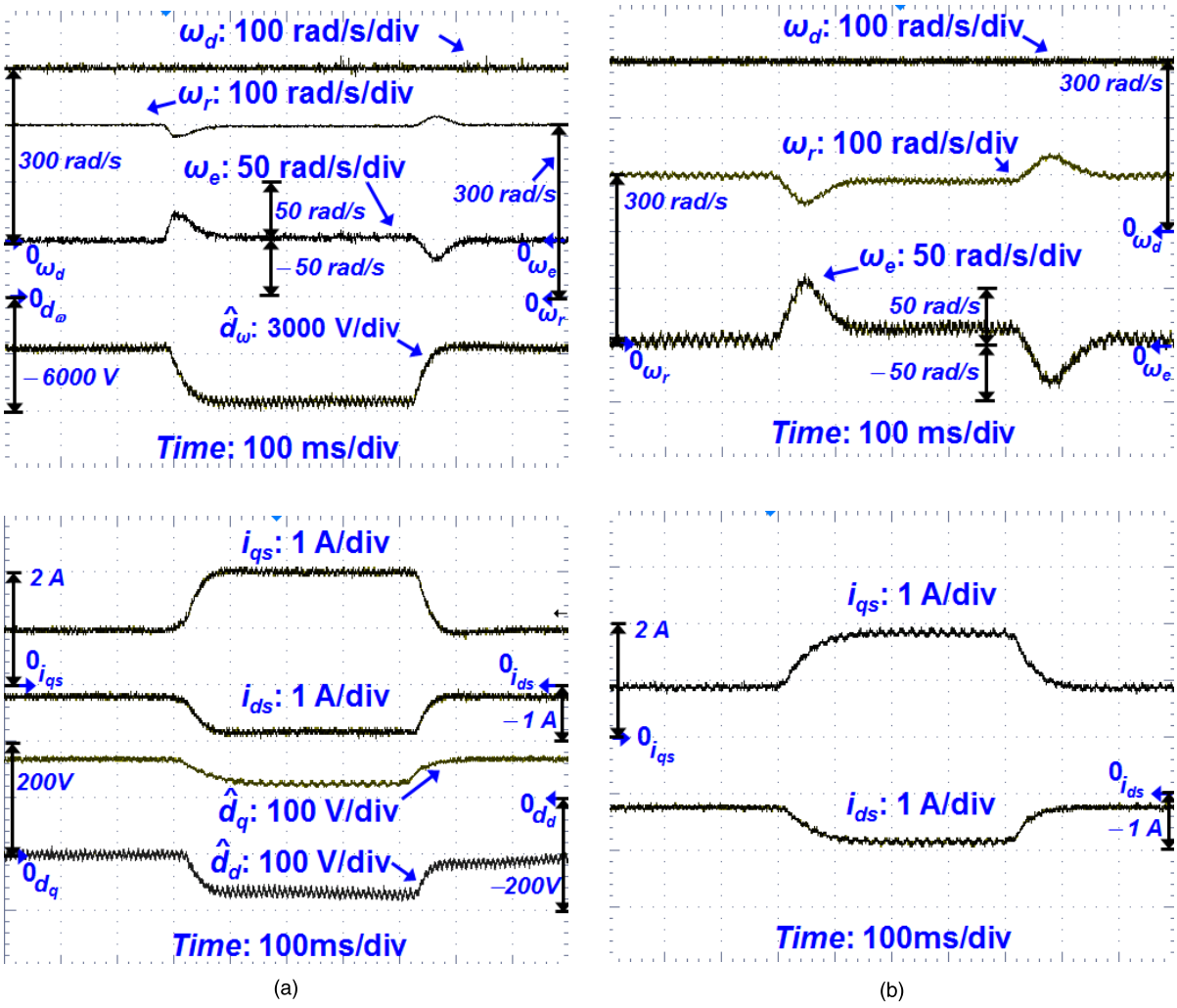

(a) (b)

FIGURE 6. Comparative experimental results under a load torque step change with parameter variations. (a) Proposed NOC ($\hat{d}_\omega$, $\hat{d}_q$, $\hat{d}_d$, ω_r, i_{ds}, and i_{qs}). (b) Conventional NOC (ω_r, i_{ds}, and i_{qs}).

among different values of N_d, the nominal values of the IPMSM parameters are changed as the staircase references in the IPMSM model at ω_r of 300 rad/s and τ_L of 1 N·m. That is, as shown in Fig. 4, the parameters of the IPMSM (i.e., L_d,L_q,R_s, λ_m, B, and J) are step-changed from the 50% (I) to the 100 % (II), and to the 150% (III) of the nominal values. It is observed in Fig. 4(i) that the convergence rates of $\hat{d}_\omega$ for $N_d = 0$, 1, 2, and 3 are 0.3, 0.12, 0.06, and 0.06 s, respectively. Similarly, the convergence rates of the $\hat{d}_q$ (0.18, 0.07, 0.05, and 0.05 s) and $\hat{d}_d$ (0.25, 0.15, 0.07, and 0.07 s) for $N_d = 0$, 1, 2, and 3 are obtained from Fig. 4(ii) and (iii), respectively. It is noted that the convergence rates for $N_d = 2$, 3 are much smaller than those for $N_d = 0$ and 1. Meanwhile, for $N_d = 2$ and 3, the $\hat{d} = [\hat{d}_\omega, \hat{d}_q, \hat{d}_d]^T$ estimated by the proposed NODO is quite similar in the step-changed regions I, II, and III. This implies that the $N_d = 2$ should be the preferable choice because of the lower computational burden compared to the $N_d = 3$. Hence, the fast convergence rate, reduced SSE, and lower computational burden shown in Fig. 4(i)−(iii) conclude that the $N_d = 2$ is the optimum number of members of the Taylor series.

On the other hand, Fig. 4(iv) presents the estimated $\hat{\tau}_{L\_Con}$ based on the conventional NODO [20], which shows the significant deviations in their estimation results owing to parameter variations. It is also observed that the SSEs of the estimated $\hat{\tau}_{L\_Con}$ due to unattended parameter variations for (I), (II), and (III) are 1, 0, and −0.4 N·m, respectively. The conventional NODO [20] reports the experimental results with 150% variations of L_{d0}, L_{q0}, and R_{s0}, but the variations in the values of λ_m, B, and J are not considered, which highly degrade the speed tracking performance. Unlike the conventional NODO [20], the proposed NODO accurately estimates the $\hat{d}$ in (3), which considers the severe variations of the L_d,L_q,R_s, λ_m, B, and J. Therefore, the proposed NODO with $N_d = 2$ shows the better disturbance attenuation performance than the conventional NODO as it can effectively estimate the disturbances due to the external load torque and parameter uncertainties.

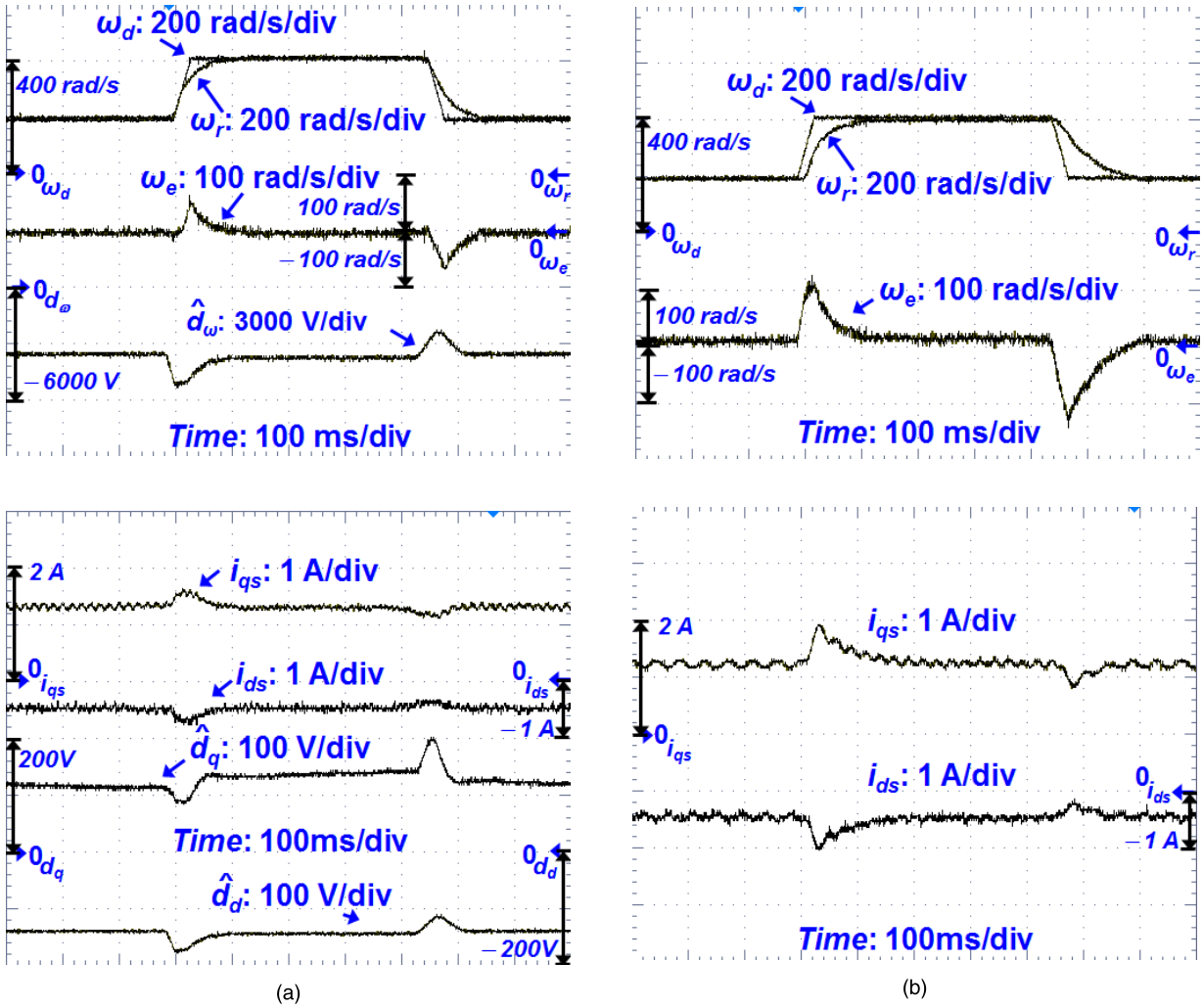

FIGURE 7. Comparative experimental results under a speed step change below rated speed with parameter variations. (a) Proposed NOC ($\hat{d}_\omega$, $\hat{d}_q$, $\hat{d}_d$, ω_r, i_{ds}, and i_{qs}). (b) Conventional NOC (ω_r, i_{ds}, and i_{qs}).

C. ROBUST TRACKING PERFORMANCE UNDER LOAD CHANGE IN THE PRESENCE OF PARAMETER VARIATIONS

In order to highlight the robust tracking performance of the proposed NOC for only external load disturbance rejection, Fig. 5 illustrates the comparative robust tracking performance of the proposed NOC compared to the conventional NOC [20] under a load step change without parameter variations. In this regard, the load torque (τ_L) is step changed from 50% rated value (0.75 N·m) to 100% rated value (1.5 N·m) while the IPMSM is running at $\omega_r = 300$ rad/s. It is observed that the ω_r of the proposed NOC ($t_s = 36$ ms; SSE = 0.5 rad/s) in Fig. 5(a) has faster and more robust tracking performance compared to the conventional NOC ($t_s = 61$ ms; SSE = 3.5 rad/s) in Fig. 5(b). It is noted that the influence of the magnetic saturation on the IPMSM under load change is compensated by adopting the $\hat{d}_\omega$ (−3588 V → −7021 V), $\hat{d}_q$ (54 V → 35 V), and $\hat{d}_d$ (−41 V → −64 V) that are estimated by the proposed NOC with the settling times (t_s) of 58 ms, 61 ms, and 32 ms, respectively. In Fig. 5(a) and (b), the proposed NOC (t_s: $i_{qs} = 65$ ms and $i_{ds} = 69$ ms) has much superior transient tracking performance of the i_{qs} and i_{ds} compared with the conventional NOC (t_s: $i_{qs} = 141$ ms and $i_{ds} = 158$ ms).

To demonstrate the performance of the proposed simplified NOC for external load disturbance rejection and insensitivity to parameter variations, Fig. 6 presents the comparative experimental results under a load torque step change with parameter variations for the proposed NOC and conventional NOC [20]. In this condition, the IPMSM runs at the steady-state ω_r of 300 rad/s and the load torque (τ_L) suddenly changes from 50% rated value (0.75 N·m) to 100% rated value (1.5 N·m) in the presence of the parameter variations, i.e., 200% for the mechanical parameters (B_0 and J_0) and 150% for the electrical parameters (i.e., L_{d0},L_{q0},R_{s0}, and λ_{m0}). Fig. 6(a) shows that the proposed NOC responds rapidly during the load change by estimating the $\hat{d}_\omega$ (−2881 V → −5519 V), $\hat{d}_q$ (169 V → 127 V), $\hat{d}_d$ (−97 V → −178 V), and ω_r with the settling times (t_s) of 91 ms, 107 ms, 83 ms,

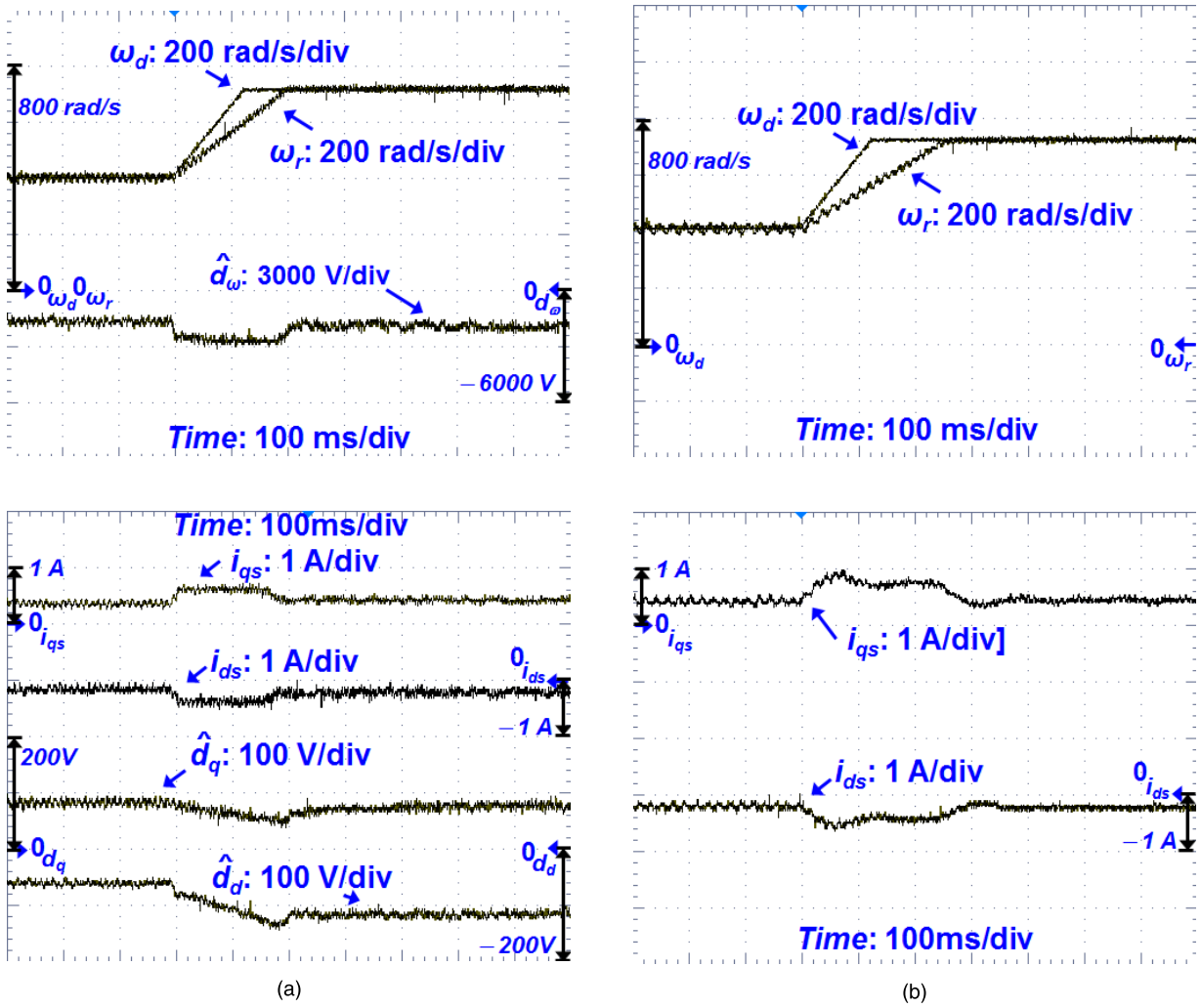

FIGURE 8. Comparative experimental results under a speed step change over wide speed range (i.e., MTPA to FW) with parameter variations. (a) Proposed NOC ($\hat{d}_\omega$, $\hat{d}_q$, $\hat{d}_d$, ω_r, i_{ds}, and i_{qs}). (b) Conventional NOC (ω_r, i_{ds}, and i_{qs}).

and 85 ms, respectively. On the other hand, the ω_r in Fig. 6(b) indicates that the conventional NOC (t_s: 145 ms) poorly suppresses the sudden changes in the external disturbances and parameter variations. The transient tracking performance of the i_{qs} and i_{ds} for the proposed NOC (t_s: $i_{qs} = 80$ ms and $i_{ds} = 89$ ms) is much better than that of the conventional NOC (t_s: $i_{qs} = 162$ ms and $i_{ds} = 178$ ms). In addition, the SSE of ω_r (Proposed: 3 rad/s, Conventional: 19 rad/s) is significantly reduced due to the utilization of $\hat{d}$ obtained from the proposed NODO.

D. ROBUST TRACKING PERFORMANCE OVER WIDE SPEED RANGE IN THE PRESENCE OF PARAMETER VARIATIONS

First, to achieve the maximum torque per ampere (MTPA) control below the rated speed (i.e., constant torque region), Fig. 7 illustrates the comparative tracking performance of the proposed NOC and conventional NOC when ω_d is step-changed from 200 to 400 rad/s and τ_L is kept at 0.75 N·m with IPMSM parameters (i.e., 200% B_0, 200% J_0, 150% L_{d0}, 150% L_{q0}, 150% R_{s0}, and 150% λ_{m0}). In this figure, the estimated disturbances $\hat{d} = [\hat{d}_\omega, \hat{d}_q, \hat{d}_d]^T$ by the proposed NODO have the fast convergence rate of 79 ms, 75ms, and 88 ms, respectively. The comparative speed response analysis of the proposed NOC and conventional NOC (settling time (t_s): 86 ms vs. 155 ms) highlights that the proposed NOC is rapid and accurate with little overshoot, establishing the robust tracking performance of the proposed controller. Besides, the transient-state response of the i_{qs} and i_{ds} for the proposed NOC (overshoot: $i_{qs} = 0.4$ A and $i_{ds} = 0.15$ A) presents significantly small overshoot, undershoot, and SSE compared to the conventional NOC (overshoot: $i_{qs} = 0.75$ A and $i_{ds} = 0.59$ A).

Next, to evaluate the robust tracking performance of the proposed NOC in the wide speed range (i.e., constant torque and flux-weakening regions), Fig. 8 shows the comparative tracking performance of the proposed NOC and conventional NOC when ω_d is commanded from 400 to 720 rad/s at the

TABLE 3. Summary of the comparative performance analysis of the proposed NOC and conventional NOC.

Operating Conditions		d_ω (V)	d_q (V)	d_d (V)	ω_e (rad/s)	t_s (ms)
Proposed NOC	Abrupt Load Change	−7021*/ −5519	35*/ 127	−64*/ −178	0.5*/ 3	36*/ 85
	Abrupt Speed Change	−3780	138	−143	56	86
	FW	−2040	75	−118	-	193

Operating Conditions		ω_e (rad/s)	t_s (ms)
Conventional NOC	Abrupt Load Change	3.5*/19	61*/145
	Abrupt Speed Change	117	155
	FW	-	272

"*" represents the operating condition without parameter variations.

light load of 0.1 N·m. In this scenario, the maximum voltage V_m in (7.b) is set to 100 V instead of 170 V to lessen the rated speed in the FW control by keeping in view of the safety of the laboratory equipment [26], [27]. Consequently, the rated speed at the $V_m = 100$ V is computed as 443 rad/s instead of 523 rad/s in Table 2 and the flux-weakening is applied above this rated speed [28]. As shown in Fig. 8(a), as the ω_r increases above the rated speed (443 rad/s) at the same load condition, the i_{dsd_FW} has to be imposed since the i_{dsd_MTPA} control is no longer feasible. Hence, the FW control is invoked with the i_{dsd_FW} attaining more negative values (-0.15 A $\rightarrow$ -0.32 A) to weaken the air gap flux. It is also observed in Fig. 8(a) that the transition between the MTPA control and FW control is very smooth, which allows a good dynamic response even at this elevated speed. In this figure, the disturbances $\hat{d}_\omega(-2040$ V), $\hat{d}_q(89$ V), and $\hat{d}_d$ (-118 V) estimated by the proposed NODO contribute to the smooth transitions between the MTPA control and FW control which verifies a good dynamic response at this elevated speed. In particular, the changes in the $\hat{d}_q$ (89 V $\rightarrow$ 75 V) and $\hat{d}_d$ (-61 V $\rightarrow$ -118 V) indicate that the proposed NODO efficiently estimates the $\hat{d}$ during the transition. Moreover, the proposed NODO accurately estimates the $\hat{d}_q$ and $\hat{d}_d$ that cover the effects of magnetic saturation (i.e., changes in the values of L_q and L_d) and are used by the proposed NOC to achieve the robustness during the FW control [27]. On the other hand, Fig. 8(b) shows that the conventional NOC has higher fluctuations with longer convergence time (272 ms) in the speed response compared to the proposed NOC (193 ms). Besides, higher fluctuations can be observed in the i_{ds} and i_{qs} waveforms. It is concluded that the proposed NOC scheme has superior control performance with the reduced CLEs compared to the conventional NOC scheme. Table 3 summarizes the comparative performance analysis of the proposed NOC and conventional NOC under the load change and wide speed range conditions.

V. CONCLUSION

This paper presents the design of a simplified NOC (i.e., NOSC and NODO) for the IPMSM drives such that the complex computations in the Taylor series for solving the SDRE are significantly reduced. During the practical implementations, the proposed NODO estimates and then compensates for the disturbances (e.g., external load torque, parameter variations, unmodeled dynamics, etc.). In this paper, the SDC of the IPMSM is restructured in order to minimize the calculation of Taylor series method and the approximate solutions of the SDRE for the proposed NOSC and NODO are easily calculated offline by solving one constant ARE and a series of CLEs. In order to prove the effectiveness of the proposed NOC technique, the comparative experimental results are presented with a TI TMS320F28335 DSP on a prototype IPMSM drive system in the wide speed range (i.e., constant torque and flux-weakening regions).

REFERENCES

[1] Y. Lee, S. H. Lee, and C. C. Chung, "LPV H∞ control with disturbance estimation for permanent magnet synchronous motors," *IEEE Trans. Ind. Electron.*, vol. 65, no. 1, pp. 488–497, Jan. 2018.

[2] V. Smidl, S. Janous, L. Adam, and Z. Peroutka, "Direct speed control of a PMSM drive using SDRE and convex constrained optimization," *IEEE Trans. Ind. Electron.*, vol. 65, no. 1, pp. 532–542, Jan. 2018.

[3] K. Liu, Z. Q. Zhu, and D. A. Stone, "Parameter estimation for condition monitoring of PMSM stator winding and rotor permanent magnets," *IEEE Trans. Ind. Electron.*, vol. 60, no. 12, pp. 5902–5913, Dec. 2013.

[4] X. Sun, L. Chen, H. Jiang, Z. Yang, J. Chen, and W. Zhang, "High-performance control for a bearingless permanent-magnet synchronous motor using neural network inverse scheme plus internal model controllers," *IEEE Trans. Ind. Electron.*, vol. 63, no. 6, pp. 3479–3488, Jun. 2016.

[5] X. Liu, H. Chen, J. Zhao, and A. Belachen, "Research on the performances of interior PMSM used for electric vehicles," *IEEE Trans. Ind. Electron.*, vol. 63, no. 6, pp. 3533–3545, Jun. 2016.

[6] J. Yang, W. H. Chen, S. Li, L. Guo, and Y. Yan, "Disturbance/uncertainty estimation and attenuation techniques in PMSM drives—A survey," *IEEE Trans. Ind. Electron.*, vol. 64, no. 4, pp. 3273–3285, Apr. 2017.

[7] X. Sun, Z. Shi, L. Chen, and Z. Yang, "Internal model control for a bearingless permanent magnet synchronous motor based on inverse system method," *IEEE Trans. Energy Convers.*, vol. 31, no. 4, pp. 1539–1548, Dec. 2016.

[8] X. Sun, B. Su, L. Chen, Z. Yang, X. Xu, and Z. Shi, "Precise control of a four degree-of-freedom permanent magnet biased active magnetic bearing system in a magnetically suspended direct-driven spindle using neural network inverse scheme," *Mech. Syst. Signal Process.*, vol. 88, pp. 36–48, May 2017.

[9] X. Sun, L. Chen, Z. Yang, and H. Zhu, "Speed-sensorless vector control of a bearingless induction motor with artificial neural network inverse speed observer," *IEEE/ASME Trans. Mechatron.*, vol. 18, no. 4, pp. 1357–1366, Aug. 2013.

[10] D. Q. Dang, M. S. Rafaq, H. H. Choi, and J. W. Jung, "Online parameter estimation technique for adaptive control applications of interior PM synchronous motor drives," *IEEE Trans. Ind. Electron.*, vol. 63, no. 3, pp. 1438–1449, Mar. 2016.

[11] M. S. Rafaq, F. Mwasilu, J. Kim, H. H. Choi, and J. W. Jung, "Online parameter identification for model-based sensorless control of interior permanent magnet synchronous machine," *IEEE Trans. Power Electron.*, vol. 32, no. 6, pp. 4631–4643, Jun. 2017.

[12] M. A. M. Cheema, J. E. Fletcher, D. Xiao, and M. F. Rahman, "A linear quadratic regulator-based optimal direct thrust force control of linear permanent-magnet synchronous motor," *IEEE Trans. Ind. Electron.*, vol. 63, no. 5, pp. 2722–2733, May 2016.

[13] M. A. M. Cheema, J. E. Fletcher, M. F. Rahman, and D. Xiao, "Optimal, combined speed, and direct thrust control of linear permanent magnet synchronous motors," *IEEE Trans. Energy Convers.*, vol. 31, no. 3, pp. 947–958, Sep. 2016.

[14] C. Xia, N. Liu, Z. Zhou, Y. Yan, and T. Shi, "Steady-state performance improvement for LQR-based PMSM drives," *IEEE Trans. Power Electron.*, vol. 33, no. 12, pp. 10622–10632, Dec. 2012. doi: 10.1109/TPEL.2018.28003760.
[15] J. S. Shamma and J. R. Cloutier, "Existence of SDRE stabilizing feedback," *IEEE Trans. Autom. Control*, vol. 48, no. 3, pp. 513–517, Mar. 2003.
[16] Y.-W. Liang and L. G. Lin, "Analysis of SDC matrices for successfully implementing the SDRE scheme," *Automatica*, vol. 49, no. 10, pp. 3120–3124, Oct. 2013.
[17] A. J. Laub and P. Gahinet, "Numerical improvements for solving Riccati equations," *IEEE Trans. Autom. Control*, vol. 42, no. 9, pp. 1303–1308, Sep. 1997.
[18] A. J. Laub, "A Schur method for solving algebraic Riccati equations," *IEEE Trans. Autom. Control*, vol. AC-24, no. 6, pp. 913–921, Dec. 1979.
[19] T. D. Do, H. H. Choi, and J. W. Jung, "SDRE-based near optimal control design for PM synchronous motor," *IEEE Trans. Ind. Electron.*, vol. 59, no. 11, pp. 4063–4074, Nov. 2012.
[20] T. D. Do, S. Kwak, H. H. Choi, and J.-W. Jung, "Suboptimal control scheme design for interior permanent-magnet synchronous motors: An SDRE-based approach," *IEEE Trans. Power Electron.*, vol. 29, no. 6, pp. 3020–3031, Jun. 2014.
[21] E. Lu, W. Li, X. Yang, and S. Xu, "Composite sliding mode control of a permanent magnet direct-driven system for a mining scraper conveyor," *IEEE Access*, vol. 5, pp. 22399–22408, Oct. 2017.
[22] G. Schoonhoven and M. N. Uddin, "MTPA- and FW-based robust nonlinear speed control of IPMSM drive using Lyapunov stability criterion," *IEEE Trans. Ind. Appl.*, vol. 52, no. 5, pp. 4365–4374, Sep./Oct. 2016.
[23] H. H. Choi, "SDRE-based near optimal nonlinear controller design for unified chaotic systems," *Nonlinear Dyn.*, vol. 70, no. 3, pp. 2063–2070, Nov. 2012.
[24] H. T. Bank, B. M. Lewis, and H. T. Tran, "Nonlinear feedback controllers and compensators: A state-dependent Riccati equation approach," *J. Comput. Optim. Appl.*, vol. 37, no. 2, pp. 177–218, Mar. 2007.
[25] F. Lin, *Robust Control Design: An optimal Control Approach*. Chichester, U.K.: Wiley, 2007.
[26] S. Morimoto, M. Sanada, and Y. Takeda, "Wide-speed operation of interior permanent magnet synchronous motors with high-performance current regulator," *IEEE Trans. Ind. Appl.*, vol. 30, no. 4, pp. 920–926, Jul. 1994.
[27] J. M. Kim and S. K. Sul, "Speed control of interior permanent magnet synchronous motor drive for the flux weakening operation," *IEEE Trans. Ind. Appl.*, vol. 33, no. 1, pp. 12–19, Jan./Feb. 1997.
[28] C.-T. Pan and S. M. Sue, "A linear maximum torque per ampere control for IPMSM drives over full-speed range," *IEEE Trans. Energy Convers.*, vol. 20, no. 2, pp. 359–366, Jun. 2005.

MUHAMMAD SAAD RAFAQ received the B.S. degree in electrical engineering from the University of Engineering and Technology, Taxila, Pakistan, in 2011. He is currently pursuing the Ph.D. degree with the Division of Electronics and Electrical Engineering, Dongguk University, Seoul, South Korea.

From 2012 to 2013, he was a Laboratory Engineer with the University of Gujrat, Gujrat, Pakistan. His research interests include distributed generation systems, electric vehicles, and DSP-based electric machine drives.

ANH TUAN NGUYEN received the B.S. and M.S. degrees in electrical engineering from the Hanoi University of Science and Technology, Hanoi, Vietnam, in 2010 and 2012, respectively, and the M.S. degree in electrical engineering from the Grenoble Institute of Technology, Joseph Fourier University, Grenoble, France, in 2015. He is currently pursuing the Ph.D. degree with the Division of Electronics and Electrical Engineering, Dongguk University, Seoul, South Korea.

His research interests include electric power systems, control of power converters, and DSP-based electric machine drives.

HAN HO CHOI (M'03) received the B.S. degree in control and instrumentation engineering from Seoul National University, Seoul, South Korea, in 1988, and the M.S. and Ph.D. degrees in electrical engineering from the Korea Advanced Institute of Science and Technology, Daejeon, South Korea, in 1990 and 1994, respectively.

He is currently with the Division of Electronics and Electrical Engineering, Dongguk University, Seoul. His research interest includes control theory and its applications to real-world problems.

JIN-WOO JUNG (M'06) received the B.S. and M.S. degrees in electrical engineering from Hanyang University, Seoul, South Korea, in 1991 and 1997, respectively, and the Ph.D. degree in electrical and computer engineering from The Ohio State University, Columbus, OH, USA, in 2005.

From 1997 to 2000, he was with the Home Appliance Research Laboratory, LG Electronics Co., Ltd., Seoul. From 2005 to 2008, he was a Senior Engineer with the R&D Center and with the PDP Development Team, Samsung SDI Co., Ltd., South Korea. Since 2008, he has been a Professor with the Division of Electronics and Electrical Engineering, Dongguk University, Seoul. His research interests include DSP-based electric machine drives, distributed generation systems using renewable energy sources, and power conversion systems and drives for electric vehicles.